



1 **Large Reductions in Satellite-Derived and Modelled European Lower Tropospheric**
2 **Ozone During and After the COVID-19 Pandemic (2020–2022)**

3
4 **Matilda. A. Pimlott¹, Richard. J. Pope^{1,2}, Brian. J. Kerridge^{3,4}, Richard. Siddans^{3,4}, Barry.**
5 **G. Latter^{3,4}, Lucy. J. Ventress^{3,4}, Wuhu. Feng^{1,5}, Martyn. P. Chipperfield^{1,2}**

6 ¹School of Earth and Environment, University of Leeds, Leeds, LS2 9JT, UK

7 ²National Centre for Earth Observation, University of Leeds, Leeds, LS2 9JT, UK

8 ³Remote Sensing Group, STFC Rutherford Appleton Laboratory, Chilton, Oxfordshire, OX11
9 0QX, UK

10 ⁴National Centre for Earth Observation, STFC Rutherford Appleton Laboratory, Chilton,
11 Oxfordshire, OX11 0QX, UK

12 ⁵National Centre for Atmospheric Science, University of Leeds, Leeds, LS2 9PH, UK

13

14 Submitted to *Atmospheric Chemistry and Physics*

15 Corresponding author: Richard J. Pope (R.J.Pope@leeds.ac.uk)

16

17 **Key Points:**

- 18 • The European satellite record shows large lower tropospheric spring-summer ozone
19 reductions in 2020–2022, of 11.0%, 8.4% and 14.6%.
- 20 • Scaling precursor emissions based on activity data yields large model ozone reductions in
21 the spring-summer of 2020 and 2021.
- 22 • In 2020, meteorology contributed ~1/3 of the modelled reduction (low stratosphere-
23 troposphere flux), with ~2/3 from emission reductions.



24 **Abstract**

25 Activity restrictions during the COVID-19 pandemic caused large reductions in ozone (O₃) precursor emissions.
26 Studies showed large O₃ reductions in the 2020 spring-summer Northern Hemisphere free troposphere coinciding
27 with this emission reduction period. Here, we provide an insight into the European satellite-derived tropospheric O₃
28 record updated to mid-2023. Rutherford Appleton Laboratory (RAL) retrieval products show large negative
29 anomalies in the spring-summer periods of 2020 – 2022, with the largest in 2022, and smaller reductions in 2023.
30 The Infrared Atmospheric Sounding Interferometer (IASI) showed peak reductions compared to monthly averages
31 of 2.2 DU (11.0%), 1.7 DU (8.4%) and 2.8 DU (14.6%) in 2020, 2021 and 2022, respectively. Scaling model
32 emissions, based on activity reduction data, yields large negative anomalies peaking in May 2020 and 2021.
33 Emissions reduction was the greater influence, explaining ~65% of the decrease, however, the meteorological
34 impact was substantial, driven by a reduced stratosphere-troposphere O₃ exchange flux.

35 **Plain Language Summary**

36 Lockdowns and other measures implemented to limit the spread of COVID-19 reduced human activity, leading to a
37 reduction in emissions from humans, including precursors for tropospheric ozone (O₃), a pollutant and greenhouse
38 gas. Studies have shown a reduction in tropospheric O₃ across the northern hemisphere in the spring-summer of
39 2020, which coincided with this emission reduction. We provide further evidence of the tropospheric O₃ reduction in
40 2020, specifically for Europe, using two records derived from satellite instruments. The two records show large
41 reductions in European tropospheric O₃ in the spring-summer of 2020, peaking at ~ 10 – 20 % in May. One record
42 continues into 2023, showing the largest reductions in 2022, the year after the initial 2020/2021 pandemic period,
43 however, the reductions are smaller in the following year of 2023. We use a chemical transport model to distinguish
44 between the impacts of emissions and meteorology in 2020–2021. In both years, emission reductions had greater
45 influence on the O₃ reduction (~2/3), highlighting the importance of emissions in decreasing O₃. However,
46 emissions reductions alone were not responsible for the large O₃ reduction, as there was considerable influence from
47 meteorology (~1/3), mostly from variation in the flux of O₃ from the stratosphere.

48 **1 Introduction**

49 Tropospheric O₃ is an important secondary atmospheric pollutant and short-lived climate forcer, formed in the
50 presence the precursor gases, nitrogen oxides (NO_x, referring to nitrogen dioxide (NO₂) and nitric oxide (NO)) and
51 volatile organic compounds (VOCs), and sunlight (P. S. Monks et al., 2015). Tropospheric O₃ is a persistent health
52 problem in Europe, with 24,000 premature deaths attributed to acute O₃ exposure in 2020 (European Environment
53 Agency, 2022). O₃ is also the 3rd most important greenhouse gas, with an estimated effective radiative forcing of
54 0.47 W m⁻² (0.24–0.71 W m⁻²) between 1750–2019, dominated by changes in tropospheric O₃ (IPCC, 2021; Skeie et
55 al., 2020).

56
57 Due to a global pandemic caused by COVID-19 (disease from SARS-CoV-2, severe acute respiratory syndrome
58 coronavirus-2), many countries worldwide implemented a ‘lockdown’ of daily life activities to prevent the spread of



59 the disease (Forster et al., 2020; WHO, 2020; Zhou et al., 2020). This resulted in a widespread reduction in
60 anthropogenic surface emissions, including O₃ precursor gases. Based on activity data, Forster et al. (2020)
61 estimated a global reduction of ~ 30% for NO_x, 25% for carbon monoxide (CO) and 20% for VOCs in April 2020
62 and Guevara et al. (2021) estimated reductions of ~ 33% for NO_x and 8% for VOCs in March/April 2020.
63 Furthermore, Guevara et al. (2021) found that countries with the severest lockdowns had even higher average
64 reductions (~ 50% for NO_x, 14% for VOCs).
65
66 Reductions in tropospheric O₃ in the spring-summer across the northern hemisphere (NH) free troposphere (FT) was
67 initially described by Steinbrecht et al. (2021). The timing of this reduction coincides with the introduction of
68 lockdowns across Europe, beginning in the spring-summer of 2020 and continuing into 2021. Steinbrecht et al.
69 (2021) found that in 2020, measurements of the NH FT (mostly from ozonesondes) from April–August showed ~7%
70 lower O₃ values, compared to its climatology of 2000–2020. Such a widespread reduction occurring at so many
71 stations had not occurred previously in this time period. Another notable event during winter-spring of 2019/2020
72 was the very large stratospheric Arctic O₃ depletion caused by a very cold, strong and long-lasting polar vortex (W.
73 Feng et al., 2021; Weber et al., 2021; Wohltmann et al., 2020). Steinbrecht et al. (2021) suggested that this low
74 stratospheric O₃ event contributed to less than 25% of this O₃ negative anomaly, attributing most of the O₃ reduction
75 to emission reductions. Further studies have confirmed low FT O₃ across Europe and the NH using aircraft and
76 ozonesonde measurements (e.g. Chang et al. (2022); Clark et al. (2021)). In contrast, Parrish et al. (2022) suggested
77 that low 2020 tropospheric O₃ could be largely due to a negative trend in baseline tropospheric O₃ since around the
78 mid-2010s, based on Western European surface sites.
79
80 From a satellite perspective, Ziemke et al. (2022) found low NH spring-summer FT O₃ from instruments aboard
81 NASA satellites, using a merged instrument record. The tropospheric column O₃ reduction of ~ 7–8% (3 DU)
82 (compared to 2016–2019), was comparatively uniform between 20°N - 60°N and repeated in the next year, 2021.
83 They found a reduction of NH satellite-derived NO₂ (~ 10–20%) in the spring-summer of 2020 and 2021, attributing
84 this as the likely cause of the O₃ reduction. Cuesta et al. (2022) found that satellite-derived lowermost tropospheric
85 O₃ (< 3 km altitude) in the spring (1st–15th April) of 2020 was enhanced across central Europe and northern Italy
86 (typically VOC-limited regions) compared to the previous year (2019) and reduced elsewhere in Europe (typically
87 NO_x-limited regions). An enhancement of O₃ across central Europe in the spring-summer of 2020 was also found at
88 surface monitoring sites (e.g. Ordóñez et al. (2020); Grange et al. (2021)). Apart from Ziemke et al. (2022), there are
89 few studies of 2021 and onwards. One example is from Pey & Cerro (2022), finding reduced background O₃ values
90 over SW Europe (~15% at most sites) in March-April 2020, which was also seen in 2021 but to a lesser extent.
91
92 Modelling studies have investigated the impact of emission reduction on FT O₃, using different methods to estimate
93 the size of these emission reductions, which are still uncertain. Bouarar et al. (2021) modelled primary pollutant
94 emission reductions, based on emission reductions from activity data by Doumbia et al. (2021), finding zonally
95 averaged NH FT O₃ to be reduced by 5–15% (2001–2019 baseline). One third of this reduction is attributed to



96 reductions in air traffic, one third is attributed to a reduction in surface emissions and the final third is attributed to
97 meteorology, including the low 2020 springtime Arctic stratospheric O₃. Miyazaki et al. (2021) used data
98 assimilation, finding a reduction in the global tropospheric O₃ burden of ~ 2% in May and June 2020.

99

100 Here, we present an update to the European tropospheric O₃ record using two satellite products, extending the record
101 to mid-2023, and present the reductions in the lower FT compared to previous years. Using a 3-D chemical transport
102 model, TOMCAT (S. A. Monks et al., 2017), we explore the impact of scaling the anthropogenic surface emissions
103 (from activity data changes) on European tropospheric O₃ in 2020 and 2021. Lastly, we quantify the relative
104 contribution of emissions and meteorology to the modelled reduction in tropospheric O₃.

105 **2 Data and Methods**

106 **2.1 Tropospheric Ozone Satellite Datasets**

107 We present satellite-derived O₃ from two satellite instruments, the Infrared Atmospheric Sounding Interferometer
108 (IASI) and the Global Ozone Monitoring Experiment-2 (GOME-2), both aboard EUMETSAT's satellite MetOp-B
109 (Clerbaux et al., 2009; Munro et al., 2016). The MetOp series of satellites have a sun-synchronous, near polar orbit
110 with an equator crossing time of 9:30 local solar time (LST). IASI has a swath width of 2200 km, and in the nadir
111 viewing mode, there are four circular fields of view across-track with a diameter of 12 km, covering a square 50 ×
112 50 km² which is scanned across the swath. IASI measures in the infrared (IR) wavelengths (645–2760 cm⁻¹) with a
113 spectral resolution of 0.3 - 0.5 cm⁻¹ (Clerbaux et al., 2009). GOME-2 measures in the ultraviolet-visible (UV-Vis)
114 wavelengths (240–790 nm) with a spectral resolution of 0.26 - 0.51 nm, and has a swath width of 1920 km. The field
115 of view is scanned across-track yielding 24 ground-pixels of dimension 80 km (across-track) × 40 km (along-track)
116 (Callies et al., 2000; Munro et al., 2016). For quality assurance, the GOME-2B record was filtered for a geometric
117 cloud fraction of <0.2 (e.g. Miles et al. (2015)) and the IASI-IMS-extended record was filtered for an effective cloud
118 fraction of <0.5 (as in Pope et al. (2021)).

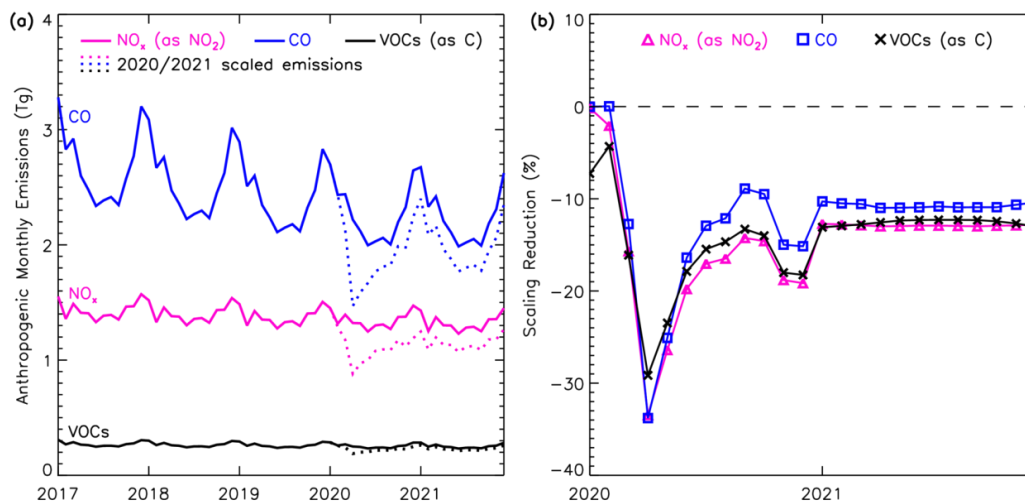
119

120 Height-resolved O₃ distributions are retrieved by the Rutherford Appleton Laboratory (RAL) using the IMS-
121 Extended scheme for IASI (detailed in Pope et al. (2021)) and UV-Vis scheme for GOME-2 (detailed in Miles et al.
122 (2015)). Due to an underlying negative tendency in the GOME-2 record, likely from UV degradation of the
123 instrument, we have detrended that record, as shown in **Supplement Text S1** and **Figure S1**. To compare the IASI-
124 IMS-Extended data from MetOp-B (2018–2023) to a longer time-period, we combine the record with IASI-IMS-
125 Extended data from MetOp-A (2008–2017). The MetOp-B record was adjusted according to monthly differences
126 with the MetOp-A record in the overlap year of 2018, as described in **Supplement Text S2** and **Figures S2 and S3**.
127 Here we use lower tropospheric sub-columns of the surface–450 hPa (~6 km altitude) derived from the retrieved
128 profiles, with a focus on Europe. As such, we use a land mask to extract a terrestrial European signal given the direct
129 link between surface O₃, precursors gases and air pollution exposure (see **Supplement Figure S4**).



130 2.2 Model Simulations

131 We use the TOMCAT 3-D chemical transport model to simulate tropospheric O₃ between 2017 and 2021. The
132 model control simulation is for 2017, 2018 and 2019. However, in 2020, the control simulation splits into two
133 scenarios: 1) business-as-usual scenario (BAU) and 2) scaled emission scenario (COVID). For the BAU scenario,
134 the control modelled emissions inventory is used but for the COVID scenario, we apply emission reduction factors
135 (Forster et al., 2020) to model surface and aircraft emissions to account for changes in activity due to the pandemic
136 in 2020 and 2021. However, COVID scaling for emissions are not available beyond 2021, so the model simulations
137 are restricted to 2017-2021. TOMCAT is an off-line model driven by 6-hourly ERA-5 meteorological reanalyses
138 (Hersbach et al., 2020), with a resolution of 2.8° × 2.8° and 31 vertical levels between the surface and 10 hPa,
139 coupled with the Global Model of Aerosol Processes (GLOMAP) (Chipperfield, 2006; Mann et al., 2010; Spracklen
140 et al., 2005). The chemistry scheme includes approximately 80 advected tracers and over 200 chemical reactions (S.
141 A. Monks et al., 2017). Surface emission fields are described in detail in **Supplement Text S4** and **Table S1**. The
142 anthropogenic emissions are from the Coupled Model Intercomparison Project Phase 6 (CMIP6) (L. Feng et al.,
143 2020), whereby after 2014 emissions are based on Shared Socioeconomic Pathways (SSPs) (Gidden et al., 2019;
144 Riahi et al., 2017). In this study, we have used the middle-of-the-road scenario, SSP2-4.5, for the TOMCAT control
145 run between 2017 and 2019, before diverging into the BAU and COVID simulations. For the BAU simulation, the
146 CMIP6 SSP2-4.5 emissions are used but for the COVID simulation, scaling factors for emission reductions from
147 national lockdowns come from Forster et al. (2020) and were applied to the BAU emissions. Forster et al. (2020)
148 used national mobility/activity data to estimate reductions in air pollutant emissions (i.e. NO_x, CO, VOCs, black
149 carbon (BC) and organic carbon (OC)). **Figure 1(a)** highlights the impacts of the scale factors, with substantial
150 decreases evident in European emissions for NO_x, CO and VOCs. **Figure 1(b)** shows that the peak reductions were
151 in April 2020, once most European lockdowns were in effect, with monthly reductions of 0.44 Tg (33%), 0.75 Tg
152 (34%) and 0.06 Tg (29%) of NO_x (as NO₂), CO and NMVOCs (as carbon (C)), respectively. For 2020, a secondary
153 winter emissions reduction occurs at ~ 15–20% as further European lockdowns were imposed to reduce the spread
154 of COVID-19. For 2021, the scaling factors from Forster et al. (2020) suggest that emissions were approximately
155 10–13% lower than expected but remained consistent throughout the year, suggesting a potential ‘new normal’ of
156 lower precursor emissions. A tracer for stratosphere-troposphere exchange (STE) in the model (O_{3S}) is used to
157 understand the impact of O₃ transport from the stratosphere. In the stratosphere, it is set equal to the model-
158 calculated O₃. The only tropospheric source of the tracer is transport from the stratosphere while its sinks are via
159 photolysis, surface deposition and reactions with HO₂, OH and H₂O through O(¹D) produced from O_{3S} (S. A. Monks
160 et al., 2017). Overall, TOMCAT is a robust and well evaluated CTM having been used in multiple studies of
161 tropospheric O₃ (e.g. Richards et al. (2013), Pope et al. (2021) and Pope et al. (2023)), thus a suitable modelling
162 framework for this study.



163

164 **Figure 1.** European aggregated anthropogenic monthly emissions of NO_x (as NO₂), CO and NMVOCs (as C) used
165 in the TOMCAT simulations between 2017 and 2021. (a) BAU emissions (solid) and COVID emissions in 2020 and
166 2021 (dotted) (Tg). (b) Percentage reduction in 2020 and 2021 for NO_x, CO and VOCs in the COVID emissions,
167 relative to the BAU emissions.

168 3 Results and Discussion

169 3.1 European Tropospheric Ozone Satellite Record (2008–2023)

170 We present two satellite-derived lower tropospheric sub-column O₃ records for continental Europe from 2008–2023
171 (**Figure 2**). During the overlapping years of 2015–2019, the records show an average difference of 2.5 DU, but the
172 variability is well correlated (Pearson’s correlation coefficient ~ 0.80). Satellite record inconsistencies are likely due
173 to differences between IR and UV-Vis instruments, the related retrieval schemes and their vertical sensitivities,
174 despite the instruments being aboard the same platform and having the same overpass time. Compared to a monthly
175 baseline of 2015–2019 for GOME-2B and 2008–2019 for IASI-IMS-Extended, the monthly anomalies (**Figure**
176 **2(b)**) show good agreement through this overlap period, with the most notable disagreements in winter/spring of
177 2015 and spring-summer 2016. Both records show large negative anomalies in spring-summer 2020. GOME-2B
178 shows peak negative anomalies of 2.4 DU (18.3%) and 3.0 DU (21.4%) in April and May 2020, respectively, and
179 IASI-IMS-Extended shows slightly smaller negative anomalies of 1.7 DU (9.4%) and 2.2 DU (11.0%) in April and
180 May, respectively. For the records shown in **Figure 2(b)**, two standard deviations (2σ) across the entire monthly
181 record is 2.1 DU for GOME-2B and 1.8 DU for IASI-IMS-Extended. Thus, ~ 95% of the data ranges between the
182 average $\pm 2\sigma$ for the respective records. In both cases, April and May 2020 negative anomalies either match or
183 surpass this range signifying relatively substantial anomalies for these months, highlighting their unusual nature.
184 The reductions continue into the summer of 2020, with both records showing large negative anomalies in July and



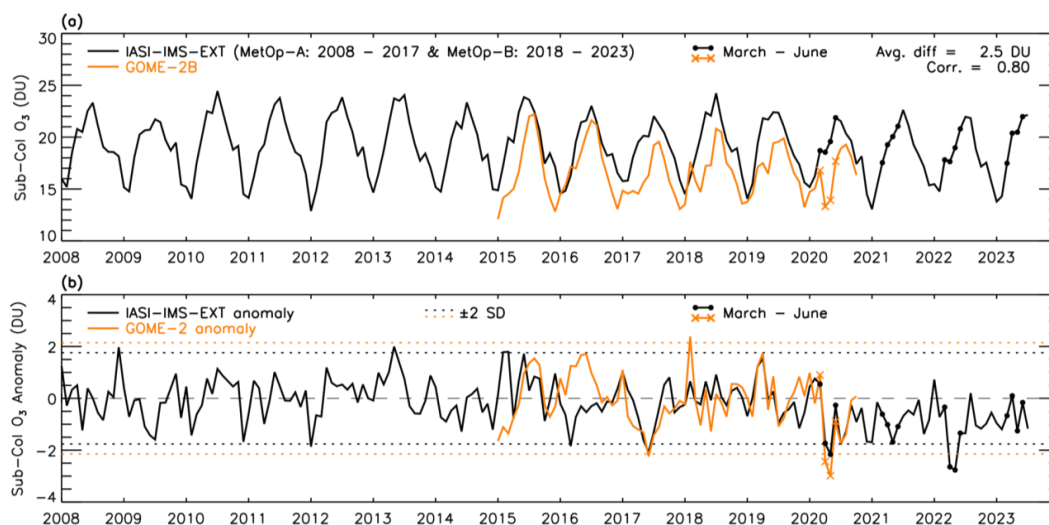
185 August: 1.7 DU (9.2%) and 1.4 DU (7.2%) for GOME-2B; 1.8 DU (8.3%) and 1.3 DU (6.3%) for IASI-IMS-
186 Extended.

187

188 Tropospheric O₃ reductions continue into the spring and summer period of 2021, with the IASI-IMS-Extended
189 record showing negative anomalies in most months of 2021, however, these anomalies are slightly smaller than in
190 2020. The largest negative anomalies are in April, May and June, at 1.0 DU (5.3%), 1.7 DU (8.4%) and 1.1 DU
191 (5.2%), respectively, with only the reduction in May being close to the average $\pm 2\sigma$ threshold. This recurrence in
192 2021 of a tropospheric O₃ reduction of similar magnitude to 2020 is consistent with the combined NASA satellite
193 product tropospheric column O₃ record for the 20-60N latitude band reported by Ziemke et al. (2022), which is
194 presented from January–August.

195

196 In 2022, the IASI-IMS-Extended record shows even larger negative anomalies in April and May than 2020/2021, of
197 2.6 DU (15.0%) and 2.8 DU (14.6%), respectively, which are well beyond the average $\pm 2\sigma$ threshold. The negative
198 anomalies continue in June and July, with 1.3 DU (6.5%) and 1.3 DU (6.1%). In 2023, the negative anomalies in
199 spring-summer are smaller compared to 2020–2022, apart from in May, where the negative anomaly is 1.3 DU
200 (6.1%). Broadly, the years of 2020–2023 all show monthly anomalies which are more consistently negative than the
201 previous 12 years. The question of the persistence of low European O₃ values will become evident in future years
202 through extension of these MetOp records.



203

204 **Figure 2.** European satellite-derived O₃ from January 2008–July 2023. (a) Monthly average sub-column (surface–
205 450 hPa) O₃ record (DU) from IASI (IASI-IMS-extended, January 2008–July 2023) and GOME-2B (January 2015–
206 October 2020). (b) Monthly mean anomalies for the two records (2015–2019 baseline for GOME-2B, 2008–2019
207 for IASI-IMS-Extended) (DU). Dotted lines indicate $\pm 2\sigma$ from the average of the record. Filled circles (IASI-IMS-
208 Extended) and crosses (GOME-2B) are shown for the months of March–June in 2020–2023, to highlight the
209 relevant spring/summer periods. Average difference and correlation are based on January 2015–December 2019.



210 3.2 TOMCAT Model Experiments (2017–2021)

211 In 2020, scaling the emissions according to the mobility data estimates in Forster et al. (2020) (TOMCAT COVID
212 scenario) caused a monthly reduction in tropospheric O₃ from March to December (**Figure 3(a)**). During January
213 and February, the COVID and BAU scenarios are very similar, however, from March onwards the COVID scenario
214 shows a negative difference compared to the BAU scenario, which peaks at 2.0 DU (8.3%) lower in May. This
215 negative difference then reduces through the year to December (0.7 DU, 4.1%). In 2021, the COVID scenario shows
216 consistent reductions in all months of the year, starting at 0.6 DU (3.4%) in January, peaking at 1.0 DU (4.3%) in
217 May, and getting slightly smaller towards the end of the year, ending with 0.6 DU (3.2%) in December. The
218 temporal pattern of the reduction is similar to the reduction in surface emissions (**Figure 1**), although with much
219 smaller percentage decreases (peak of ~30% for surface emissions and ~8% for the resulting O₃ sub-column). This
220 highlights the large emission reductions required for a sizeable reduction in European tropospheric O₃.

221
222 To identify the impact of meteorology in 2020, the scaled emissions in 2020 were used in three separate simulations
223 with the meteorology of 2017, 2018 and 2019, with an average of these three scaled emission simulations shown in
224 **Figure 3(b)**. The 2020 COVID scenario record is broadly lower than the 2017/2018/2019 averaged scaled emission
225 scenario, despite using the same surface emissions, which indicates that the meteorology of 2020 had a large impact
226 on the tropospheric O₃ reduction. The impact of meteorology in 2020 is greatest in the spring-summer, as the
227 differences between these two timeseries is largest from February–July, peaking at a 1.1 DU difference in May. This
228 demonstrates the importance of meteorology to the resulting O₃ in the spring-summer of 2020. The records are much
229 more consistent from August to the end of the year, with absolute differences below 0.6 DU, indicating a reduced
230 impact from meteorology in the second half of the year.

231
232 In comparison with the previous 3 years (2017–2019), the BAU scenario in 2020 and 2021 has lower peak spring-
233 summer values of O₃, especially compared to the high O₃ values in 2019 (**Figure 3(a)**). The spring-summer of 2020
234 shows negative anomalies in the BAU scenario of up to 1.4 DU (-5.8%) (**Figure 3(c)**). April, May and July show the
235 largest reductions, which are around the value of the average $\pm 2\sigma$ threshold (± 1.3 DU, 6.2%). The spring-summer
236 BAU scenario reductions are repeated in 2021 from January–June, peaking at 1.2 DU (4.9%) in May. Any variation
237 in the BAU scenario is due to meteorology and also variation in the BAU surface emissions used. As shown in
238 **Figure 1**, the BAU emissions only vary by a small amount from year to year, e.g. the average total annual
239 anthropogenic emission difference between consecutive years across the simulation time period is 0.33 Tg (2.0%)
240 for NO_x, 1.3 Tg (4.4%) for CO and 0.06 Tg (1.8%) for VOCs. With consistent BAU emissions, meteorology is the
241 dominant control in the BAU scenario and had a large impact on the simulated tropospheric O₃ in the spring and
242 summer of 2020.

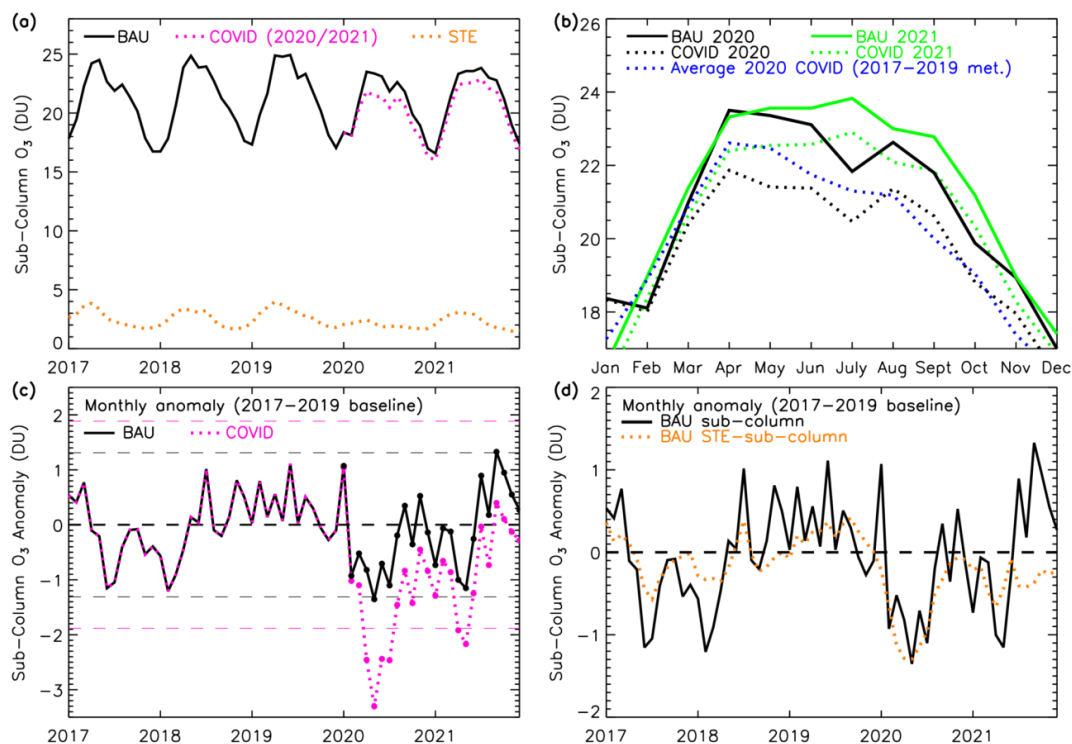
243
244 The COVID scenario shows large negative anomalies in 2020, peaking at 3.3 DU (15.4%) in May 2020 (**Figure 3c**),
245 which is much more than the average $\pm 2\sigma$ threshold (± 1.9 DU, 9.0%). Comparing the BAU and COVID scenarios
246 suggests that ~1 DU of the negative anomaly is due to meteorology (and small variations in BAU emissions) and the



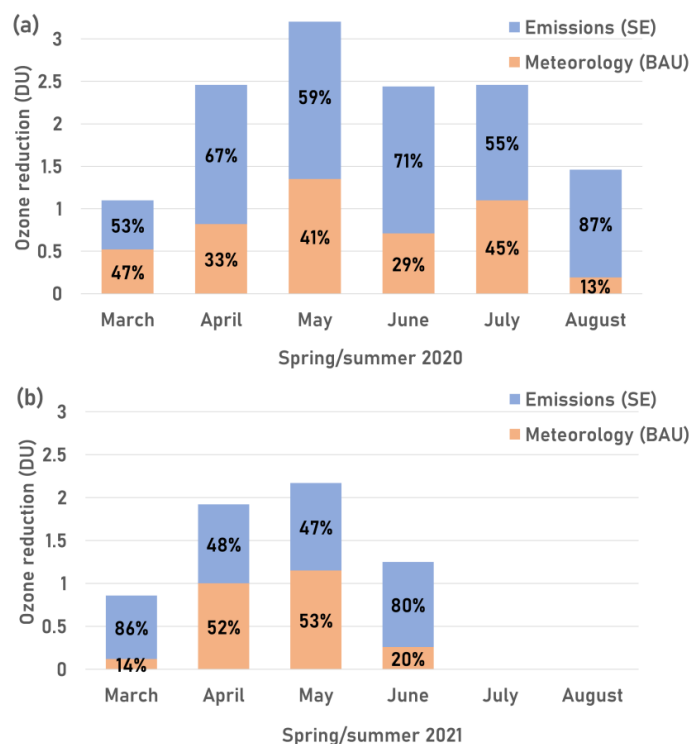
247 remaining contribution (~ 1–2 DU in spring-summer) of the negative anomaly is due to the scaled emissions for
248 2020. To further quantify the relative contributions, the difference between the anomalies for the BAU and COVID
249 scenario as a relative percentage of the COVID scenario for 2020 (i.e. $100 \times (\text{BAU} - \text{COVID})/\text{COVID}$) is shown in
250 **Figure 4(a)**. We performed this quantification for spring-summer months showing a negative anomaly in both
251 scenarios (March–August 2020 and March–June 2021). These values represent the contribution of the emission
252 reduction to the negative anomalies seen in the COVID scenario, and the corresponding contribution of meteorology
253 (and small differences in the BAU emissions). The contribution of emissions to the COVID scenario in spring-
254 summer 2020 is 53% (March), 67% (April), 59% (May), 71% (June), 55% (July) and 87% (August), with an
255 average of 65% across these months. Therefore, scaling the emissions is the dominant influence during this period.
256 In 2021, the COVID scenario also shows large negative anomalies, peaking at 2.2 DU (9.6%) in May. Scaling the
257 emissions contributed towards 86%, 48%, 47% and 80% for March–June, respectively, of the scaled negative
258 anomaly (average of 65%), with the rest due to meteorology (and BAU emissions).

259

260 The contribution of O₃ from STE to the troposphere in the model sub-column is calculated by TOMCAT as a tracer
261 which represents stratospheric O₃ that has entered the troposphere and is controlled by tropospheric sink processes.
262 We calculate a sub-column based on this contribution (STE-sub-column), shown in **Figure 3(a)**, varying between
263 1.5–4.0 DU from 2017–2021. We find a large negative anomaly in model stratosphere-troposphere O₃ exchange
264 (STE) in the spring-summer of 2020 (**Figure 3(d)**), of 1.3 DU in both April and May (52.5% and 60.5%,
265 respectively). The STE-sub-column absolute negative anomaly is a similar value or larger than the lower
266 tropospheric sub-column anomaly from March - August in 2020, suggesting that during this period, low STE
267 contribution was a substantial factor in the BAU scenario lower tropospheric sub-column O₃ reduction. In the
268 months where the STE-sub-column absolute anomaly is larger than the BAU anomaly, the other controlling factors
269 in the BAU simulation O₃ are likely around neutral or even slightly positive. The stratospheric O₃ used in the model
270 simulation is a climatology, therefore, any variation on the STE contribution is from variation in the STE flux. In
271 2021, the negative anomaly in STE-sub-column is smaller than for 2020, reaching a peak value of 0.7 DU (21.5%)
272 in April (**Figure 3(d)**). The STE-sub-column negative anomaly is also not larger than for the lower tropospheric
273 sub-column in 2021, suggesting that the STE reduction had a smaller impact on the negative lower tropospheric sub-
274 column anomalies seen in 2021, in comparison with 2020.



275
 276 **Figure 3.** TOMCAT European lower tropospheric sub-column O₃ (surface–450 hPa) between 2017 and 2021 (DU).
 277 (a) Monthly sub-column O₃ averages for the BAU sub-column (solid, black) and STE-contribution sub-column
 278 (dotted, orange). The COVID scenario is shown in 2020 and 2021 (pink dotted). (b) BAU (solid, black) and COVID
 279 scenario (dotted) records for 2020 (black), 2021 (green), with the 2017/2018/2019 averaged COVID scenario (2020
 280 scaled emissions, dark blue, dotted). (c) BAU (solid, black) and COVID (pink, dotted) O₃ anomalies (baseline of
 281 2017–2019). Horizontal dashed lines indicate $\pm 2\sigma$ from the average of the record. (d) As panel (c) with the inclusion
 282 of monthly O₃ anomalies of the STE-contribution sub-column (orange, dotted).
 283



284
285 **Figure 4.** Contribution of scaled emissions and meteorology/BAU emissions to the TOMCAT lower tropospheric
286 sub-column O₃ reduction from March–August in (a) 2020 and (b) 2021. The total reduction (DU) is the COVID
287 scenario negative anomaly, with the relative contribution of meteorology/BAU emissions shown in orange and the
288 contribution of scaled emissions shown in blue. The percentage relative contribution is labelled onto each bar
289 section.

290 **4 Conclusions**

291 Our study represents the first extended investigation of the COVID-19 pandemic impacts on European lower
292 tropospheric O₃ (surface-450 hPa) up to mid-2023. Satellite records show a substantially prolonged European
293 average decrease in spring-summer lower tropospheric in 2020, 2021 and 2022 (and to a lesser extent in 2023)
294 peaking at ~ 1.5–3.0 DU. Modelled reductions, using scaled emissions in the TOMCAT CTM to account for
295 changes in precursor trace gas emissions, are consistent for 2020 and 2021. The simulations showed that in
296 April/May 2020, ~2/3 of the negative anomaly could be attributed to scaling the emissions, with the remaining
297 reduction being attributed to meteorological processes; largely through a reduction in the flux of stratospheric O₃
298 into the troposphere. Further investigation is required to quantify the drivers of the large 2022 reductions in
299 tropospheric O₃, which could be meteorological variability and/or the stabilisation of emissions below pre-2020
300 levels (i.e. a new normal in human activity post-COVID).

301

302



303 **Acknowledgements**

304 This work was funded by the UK Natural Environment Research Council (NERC) by providing funding for the
305 National Centre for Earth Observation (NCEO, award reference NE/R016518/1) and the NERC Panorama Doctoral
306 Training Programme (DTP, award reference 580 NE/S007458/1). The TOMCAT runs were undertaken on ARC3,
307 part of the High-Performance Computing facilities at the University of Leeds, UK.

308 **Data Availability**

309 The IASI-IMS and GOME-2 data is available via the NERC Centre for Environmental Data Analysis (CEDA)
310 Jasmin platform subject to data requests. However, the IASI-IMS data and TOMCAT simulations used in this study
311 are available on Zenodo at <https://zenodo.org/records/10424302> (Pimlott et al., 2024).

312 **Author Contributions**

313 MAP and RJP conceptualised, planned and undertook the research study. BJK, RS, BGL and LJV provided the data
314 and advice on using the products. MAP performed the TOMCAT model simulations with support from MPC and
315 WF. MAP prepared the manuscript with contributions from all co-authors.

316 **Conflicts of Interest**

317 The authors declare no conflicts of interest.

318

319 **References**

- 320 Bouarar, I., Gaubert, B., Brasseur, G. P., Steinbrecht, W., Doumbia, T., Tilmes, S., et al. (2021). Ozone
321 Anomalies in the Free Troposphere During the COVID-19 Pandemic. *Geophysical Research*
322 *Letters*, 48(16), 1–11. <https://doi.org/10.1029/2021GL094204>
- 323 Callies, J., Corpaccioli, E., Eisinger, M., Hahne, A., & Lefebvre, A. (2000). GOME-2-Metop's second-
324 generation sensor for operational ozone monitoring. *ESA Bulletin*, 102(may), 28–36.
- 325 Chang, K. L., Cooper, O. R., Gaudel, A., Allaart, M., Ancellet, G., Clark, H., et al. (2022). Impact of the
326 COVID-19 Economic Downturn on Tropospheric Ozone Trends: An Uncertainty Weighted Data
327 Synthesis for Quantifying Regional Anomalies Above Western North America and Europe. *AGU*
328 *Advances*, 3(2). <https://doi.org/10.1029/2021AV000542>
- 329 Chipperfield, M. P. (2006). New version of the TOMCAT/SLIMCAT off-line chemical transport model:
330 Intercomparison of stratospheric tracer experiments. *Quarterly Journal of the Royal Meteorological*
331 *Society*, 132(617), 1179–1203. <https://doi.org/10.1256/qj.05.51>
- 332 Clark, H., Bennouna, Y., Tsvilidou, M., Wolff, P., Sauvage, B., Barret, B., et al. (2021). The effects of the
333 COVID-19 lockdowns on the composition of the troposphere as seen by In-service Aircraft for a
334 Global Observing System (IAGOS) at Frankfurt. *Atmospheric Chemistry and Physics*, 21(21),
335 16237–16256. <https://doi.org/10.5194/acp-21-16237-2021>
- 336 Clerbaux, C., Boynard, A., Clarisse, L., George, M., Hadji-Lazaro, J., Herbin, H., et al. (2009).



- 337 Monitoring of atmospheric composition using the thermal infrared IASI/MetOp sounder.
338 *Atmospheric Chemistry and Physics*, 9(16), 6041–6054. <https://doi.org/10.5194/acp-9-6041-2009>
- 339 Cuesta, J., Costantino, L., Beekmann, M., Siour, G., Menut, L., Bessagnet, B., et al. (2022). Ozone
340 pollution during the COVID-19 lockdown in the spring of 2020 over Europe, analysed from satellite
341 observations, in situ measurements, and models. *Atmospheric Chemistry and Physics*, 22(7), 4471–
342 4489. <https://doi.org/10.5194/acp-22-4471-2022>
- 343 Doumbia, T., Granier, C., Elguindi, N., Bouarar, I., Darras, S., Brasseur, G., et al. (2021). Changes in
344 global air pollutant emissions during the COVID-19 pandemic: A dataset for atmospheric modeling.
345 *Earth System Science Data*, 13(8), 4191–4206. <https://doi.org/10.5194/essd-13-4191-2021>
- 346 European Environment Agency. (2022). *Air quality in Europe 2022*. <https://doi.org/10.2800/488115>
- 347 Feng, L., Smith, S. J., Braun, C., Crippa, M., Gidden, M. J., Hoesly, R., et al. (2020). The generation of
348 gridded emissions data for CMIP6. *Geoscientific Model Development*, 13(2), 461–482.
349 <https://doi.org/10.5194/gmd-13-461-2020>
- 350 Feng, W., Dhomse, S. S., Arosio, C., Weber, M., Burrows, J. P., Santee, M. L., & Chipperfield, M. P.
351 (2021). Arctic Ozone Depletion in 2019/20: Roles of Chemistry, Dynamics and the Montreal
352 Protocol. *Geophysical Research Letters*, 48(4), 1–10. <https://doi.org/10.1029/2020GL091911>
- 353 Forster, P. M., Forster, H. I., Evans, M. J., Gidden, M. J., Jones, C. D., Keller, C. A., et al. (2020). Current
354 and future global climate impacts resulting from COVID-19. *Nature Climate Change*, 10(10), 913–
355 919. <https://doi.org/10.1038/s41558-020-0883-0>
- 356 Gidden, M. J., Riahi, K., Smith, S. J., Fujimori, S., Luderer, G., Kriegler, E., et al. (2019). Global
357 emissions pathways under different socioeconomic scenarios for use in CMIP6: a dataset of
358 harmonized emissions trajectories through the end of the century. *Geoscientific Model Development*,
359 12(4), 1443–1475. <https://doi.org/10.5194/gmd-12-1443-2019>
- 360 Grange, S. K., Lee, J. D., Drysdale, W. S., Lewis, A. C., Hueglin, C., Emmenegger, L., & Carslaw, D. C.
361 (2021). COVID-19 lockdowns highlight a risk of increasing ozone pollution in European urban
362 areas. *Atmospheric Chemistry and Physics*, 21(5), 4169–4185. [https://doi.org/10.5194/acp-21-4169-](https://doi.org/10.5194/acp-21-4169-2021)
363 2021
- 364 Guevara, M., Jorba, O., Soret, A., Petetin, H., Bowdalo, D., Serradell, K., et al. (2021). Time-resolved
365 emission reductions for atmospheric chemistry modelling in Europe during the COVID-19
366 lockdowns. *Atmospheric Chemistry and Physics*, 21(2), 773–797. [https://doi.org/10.5194/acp-21-](https://doi.org/10.5194/acp-21-773-2021)
367 773-2021
- 368 Hersbach, H., Bell, B., Berrisford, P., Hirahara, S., Horányi, A., Muñoz-Sabater, J., et al. (2020). The
369 ERA5 global reanalysis. *Quarterly Journal of the Royal Meteorological Society*, 146(730), 1999–
370 2049. <https://doi.org/10.1002/qj.3803>



- 371 IPCC. (2021). *Climate Change 2021: The Physical Science Basis: Contribution of Working Group I to*
372 *the Sixth Assessment Report of the Intergovernmental Panel on Climate Change*. (V. Masson-
373 Delmotte, P. Zhai, A. Pirani, S. L. Connors, C. Péan, S. Berger, et al., Eds.). Cambridge, United
374 Kingdom: Cambridge University Press. <https://doi.org/10.1017/9781009157896>
- 375 Mann, G. W., Carslaw, K. S., Spracklen, D. V., Ridley, D. A., Manktelow, P. T., Chipperfield, M. P., et
376 al. (2010). Description and evaluation of GLOMAP-mode: A modal global aerosol microphysics
377 model for the UKCA composition-climate model. *Geoscientific Model Development*, 3(2), 519–551.
378 <https://doi.org/10.5194/gmd-3-519-2010>
- 379 Miles, G. M., Siddans, R., Kerridge, B. J., Latter, B. G., & Richards, N. A. D. (2015). Tropospheric ozone
380 and ozone profiles retrieved from GOME-2 and their validation. *Atmospheric Measurement*
381 *Techniques*, 8(1), 385–398. <https://doi.org/10.5194/amt-8-385-2015>
- 382 Miyazaki, K., Bowman, K., Sekiya, T., Takigawa, M., Neu, J. L., Sudo, K., et al. (2021). Global
383 tropospheric ozone responses to reduced NO_x emissions linked to the COVID-19 worldwide
384 lockdowns. *Science Advances*, 7(24), 1–15. <https://doi.org/10.1126/sciadv.abf7460>
- 385 Monks, P. S., Archibald, A. T., Colette, A., Cooper, O., Coyle, M., Derwent, R., et al. (2015).
386 Tropospheric ozone and its precursors from the urban to the global scale from air quality to short-
387 lived climate forcer. *Atmospheric Chemistry and Physics*, 15(15), 8889–8973.
388 <https://doi.org/10.5194/acp-15-8889-2015>
- 389 Monks, S. A., Arnold, S. R., Hollaway, M. J., Pope, R. J., Wilson, C., Feng, W., et al. (2017). The
390 TOMCAT global chemical transport model v1.6: Description of chemical mechanism and model
391 evaluation. *Geoscientific Model Development*. <https://doi.org/10.5194/gmd-10-3025-2017>
- 392 Munro, R., Lang, R., Klaes, D., Poli, G., Retscher, C., Lindstrot, R., et al. (2016). The GOME-2
393 instrument on the Metop series of satellites: Instrument design, calibration, and level 1 data
394 processing - An overview. *Atmospheric Measurement Techniques*, 9(3), 1279–1301.
395 <https://doi.org/10.5194/amt-9-1279-2016>
- 396 Ordóñez, C., Garrido-Perez, J. M., & García-Herrera, R. (2020). Early spring near-surface ozone in
397 Europe during the COVID-19 shutdown: Meteorological effects outweigh emission changes.
398 *Science of the Total Environment*, 747(December 2019), 141322.
399 <https://doi.org/10.1016/j.scitotenv.2020.141322>
- 400 Parrish, D. D., Derwent, R. G., Faloon, I. C., & Mims, C. A. (2022). Technical note: Northern
401 midlatitude baseline ozone - Long-term changes and the COVID-19 impact. *Atmospheric Chemistry*
402 *and Physics*, 22(20), 13423–13430. <https://doi.org/10.5194/acp-22-13423-2022>
- 403 Pey, J., & Cerro, J. C. (2022). Reasons for the observed tropospheric ozone weakening over south-
404 western Europe during COVID-19: Strict lockdown versus the new normal. *Science of the Total*



- 405 *Environment*, 833(March). <https://doi.org/10.1016/j.scitotenv.2022.155162>
- 406 Pimlott, M. A., Pope, R. J., Kerridge, B. J., Siddans, R., Latter, B. G., Ventress, L. J., et al. (2024).
407 TOMCAT model data & IASI/GOME-2B satellite data of European ozone between 2008 - 2023.
408 Zenodo. <https://doi.org/doi.org/10.5281/zenodo.10424302>
- 409 Pope, R J, Kerridge, B. J., Chipperfield, M. P., Siddans, R., Latter, B. G., Ventress, L. J., et al. (2023).
410 Investigation of the summer 2018 European ozone air pollution episodes using novel satellite data
411 and modelling. *Atmospheric Chemistry and Physics*, 23(20), 13235–13253.
412 <https://doi.org/10.5194/acp-23-13235-2023>
- 413 Pope, Richard J., Kerridge, B. J., Siddans, R., Latter, B. G., Chipperfield, M. P., Arnold, S. R., et al.
414 (2021). Large enhancements in southern hemisphere satellite-observed trace gases due to the
415 2019/2020 Australian wildfires. *Journal of Geophysical Research: Atmospheres*, 1–13.
416 <https://doi.org/10.1029/2021jd034892>
- 417 Riahi, K., van Vuuren, D. P., Kriegler, E., Edmonds, J., O’Neill, B. C., Fujimori, S., et al. (2017). The
418 Shared Socioeconomic Pathways and their energy, land use, and greenhouse gas emissions
419 implications: An overview. *Global Environmental Change*, 42, 153–168.
420 <https://doi.org/https://doi.org/10.1016/j.gloenvcha.2016.05.009>
- 421 Richards, N. A. D., Arnold, S. R., Chipperfield, M. P., Miles, G., Rap, A., Siddans, R., et al. (2013). The
422 Mediterranean summertime ozone maximum: Global emission sensitivities and radiative impacts.
423 *Atmospheric Chemistry and Physics*, 13(5), 2331–2345. <https://doi.org/10.5194/acp-13-2331-2013>
- 424 Skeie, R. B., Myhre, G., Hodnebrog, Ø., Cameron-Smith, P. J., Deushi, M., Hegglin, M. I., et al. (2020).
425 Historical total ozone radiative forcing derived from CMIP6 simulations. *Npj Climate and
426 Atmospheric Science*, 3(1). <https://doi.org/10.1038/s41612-020-00131-0>
- 427 Spracklen, D. V., Pringle, K. J., Carslaw, K. S., Chipperfield, M. P., & Mann, G. W. (2005). A global off-
428 line model of size-resolved aerosol microphysics: I. Model development and prediction of aerosol
429 properties. *Atmospheric Chemistry and Physics*, 5(8), 2227–2252. [https://doi.org/10.5194/acp-5-
430 2227-2005](https://doi.org/10.5194/acp-5-2227-2005)
- 431 Steinbrecht, W., Kubistin, D., Plass-Dülmer, C., Davies, J., Tarasick, D. W., Von Der Gathen, P., et al.
432 (2021). COVID-19 Crisis Reduces Free Tropospheric Ozone Across the Northern Hemisphere.
433 *Geophysical Research Letters*, 48(5), 1–11. <https://doi.org/10.1029/2020GL091987>
- 434 Weber, M., Arosio, C., Feng, W., Dhomse, S. S., Chipperfield, M. P., Meier, A., et al. (2021). The
435 Unusual Stratospheric Arctic Winter 2019/20: Chemical Ozone Loss From Satellite Observations
436 and TOMCAT Chemical Transport Model. *Journal of Geophysical Research: Atmospheres*, 126(6),
437 1–14. <https://doi.org/10.1029/2020JD034386>
- 438 WHO. (2020). Naming the coronavirus disease (COVID-19) and the virus that causes it. Retrieved April



439 14, 2023, from [https://www.who.int/emergencies/diseases/novel-coronavirus-2019/technical-](https://www.who.int/emergencies/diseases/novel-coronavirus-2019/technical-guidance/naming-the-coronavirus-disease-(covid-2019)-and-the-virus-that-causes-it)
440 [guidance/naming-the-coronavirus-disease-\(covid-2019\)-and-the-virus-that-causes-it](https://www.who.int/emergencies/diseases/novel-coronavirus-2019/technical-guidance/naming-the-coronavirus-disease-(covid-2019)-and-the-virus-that-causes-it)
441 Wohltmann, I., von der Gathen, P., Lehmann, R., Maturilli, M., Deckelmann, H., Manney, G. L., et al.
442 (2020). Near-Complete Local Reduction of Arctic Stratospheric Ozone by Severe Chemical Loss in
443 Spring 2020. *Geophysical Research Letters*, 47(20). <https://doi.org/10.1029/2020GL089547>
444 Zhou, P., Yang, X. Lou, Wang, X. G., Hu, B., Zhang, L., Zhang, W., et al. (2020). A pneumonia outbreak
445 associated with a new coronavirus of probable bat origin. *Nature*, 579(7798), 270–273.
446 <https://doi.org/10.1038/s41586-020-2012-7>
447 Ziemke, J. R., Kramarova, N. A., Frith, S. M., Huang, L. K., Haffner, D. P., Wargan, K., et al. (2022).
448 NASA Satellite Measurements Show Global-Scale Reductions in Free Tropospheric Ozone in 2020
449 and Again in 2021 During COVID-19. *Geophysical Research Letters*, 49(15).
450 <https://doi.org/10.1029/2022GL098712>